β-Cyclodextrin-Assisted Synthesis of Superparamagnetic Magnetite Nanoparticles from a Single Fe(III) Precursor

ARTICLE *in* THE JOURNAL OF PHYSICAL CHEMISTRY C · OCTOBER 2008

Impact Factor: 4.77 · DOI: 10.1021/jp805724s

7 AUTHORS, INCLUDING:

Fuxiang Zhang
Nankai University
30 PUBLICATIONS **993** CITATIONS
SEE PROFILE

Landong Li
Nankai University
100 PUBLICATIONS **1,467** CITATIONS
SEE PROFILE

Guangjun Wu
Nankai University
58 PUBLICATIONS **721** CITATIONS
SEE PROFILE

β-Cyclodextrin-Assisted Synthesis of Superparamagnetic Magnetite Nanoparticles from a Single Fe(III) Precursor

Xiaohong Sun, Chunming Zheng, Fuxiang Zhang, Landong Li, Yali Yang, Guangjun Wu, and Naijia Guan*

Key Laboratory of Functional Polymer Materials, Department of Materials Chemistry, College of Chemistry, Nankai University, Tianjin 300071, People's Republic of China

Received: June 30, 2008; Revised Manuscript Received: September 6, 2008

A novel and facile β-cyclodextrin-assisted method has been employed in this study to prepare superparamagnetic Fe_3O_4 nanoparticles from a single iron precursor of $FeCl_3 \cdot 6H_2O$. Various characterization involving X-ray diffraction (XRD), standard and high-resolution transmission electron microscopy (TEM and HRTEM), electron diffraction (ED), and Raman spectroscopy has integrally testified the formation of pure magnetite nanoparticles with homogeneous morphology. The size of nanoparticles can be adjusted from 4 to 17 nm by varying the concentration of β-cyclodextrins. The success is ascribed to in situ formation of reducing sugar originating from the self-decomposition of β-CD under the reaction conditions, which partly reduces Fe^{3+} ions into Fe^{2+} ions for final formation of Fe_3O_4. Another function of β-CD is also discussed: that it acts as a coating agent to prevent particle growth and agglomeration, which allows the formation of nanoscale and superparamagnetic magnetite with different particle sizes. The saturation magnetization (M_s) of the as-obtained magnetite is measured and is strongly related to the particle size.

1. Introduction

Magnetic iron oxide nanoparticles have been widely studied because of their unique and tunable magnetic properties.[1,2] Nanoscale magnetite (Fe_3O_4) as one important phase of iron oxide has been extensively used in many traditional magnetic application areas, such as magnetic ferrofluids,[3] energy storage,[4] and catalysts,[5] and also holds great potential for biotechnology and biomedical research: for example, labeling and separation of various biological species,[6] magnetic resonance imaging (MRI),[7] guided drug delivery,[8] and clinical diagnosis.[9] So far, various approaches have been employed to produce pure nanoscale magnetite in order to obtain expected magnetic properties. They mainly contain coprecipitation of aqueous Fe^{2+}/Fe^{3+} salt solution by the addition of a base,[10] microemulsion technique,[11] ultrasound approach,[12] and hydrothermal synthesis.[13,14] In addition, the thermal decomposition of an organic iron precursor including $FeCup_3$,[15] $Fe(CO)_5$,[16] $Fe(acac)_3$,[17,18] or $Fe(oleate)_2$[19] at high temperature was widely used to prepare high-quality iron oxide nanoparticles with good size and morphology control.

One challenge for synthesis of nanomagnetite lies in control of the particle size and thus achieving a narrow particle size distribution. The blocking temperature of the magnetic particles depends strongly on particle size, and a wide particle size distribution will result in a wide range of blocking temperatures, leading to nonideal magnetic behavior for many applications.[1] A short burst of nucleation and subsequent slow controlled growth is known to be crucial to produce monodisperse particles. Recently, significant advances in preparing monodisperse magnetite nanoparticles of different sizes have been made by the use of organic additives as stabilization agents.[11,18,19] The other challenge for synthesis of nanomagnetite is to maintain the coexistence of Fe^{2+} ions and Fe^{3+} ions in fixed proportion (1:2) in the Fe_3O_4 structure and prevent them from being reoxidized. Purgation or protection with nitrogen[10,17,18] or argon[11,12,15,16,19] has been used widely and shown to be feasible. However, it is relatively complicated and expensive to carry out. Moreover, adding of reducing agents was also used to prohibit the ferrous ions in Fe_3O_4 from being reoxidized to ferric ions.[20] However, most of the available reducing agents, such as hydrazine, sodium borohydride ($NaBH_4$), polyol [ethylene glycol or poly(ethylene glycol)], and dimethylformamide (DMF), are potential environmental and biological risks.[21]

Another problem faced in the formation of nanomagnetite is that nanoscale particles with a large surface-to-volume ratio will cause aggregation during particle formation through van der Waals interparticle attractions.[22] A considerable amount of successful work has been reported to inhibit the aggregation by employing different coating agents, which can attach to the surface of the particles and provide spatial isolation in the synthesis system,[23] and at the same time the surface-coated magnetic nanoparticles will be more easily further modified with other functional groups or materials to extend their application in biotechnology or biomedicine fields. However, most of the reported surfactants such as linoleic acid,[13] oleylamine,[17] and oleic acid[19] are environmental concerns and also seriously limit the biomedical applications of the magnetic nanoparticles. Therefore, it seems extremely desirable to exploit a facile, economical, and environmentally friendly approach for the synthesis of pure magnetite nanoparticles.

CD (cyclodextrins) are cyclic oligosaccharides that are made up of D-glucose units (monomers) arranged in a circle (6 units = α-CD, 7 units = β-CD, 8 units = γ-CD), which are characterized by a hydrophilic exterior and a hydrophobic interior.[24] It is environmentally friendly and commonly used in the food industry. The identities of encapsulating organic molecules and self-assembly have led to intensive studies of CD and their inclusion complexes.[25] Many nanostructural compounds and composites have been constructed by the self-

* To whom correspondence should be addressed: tel 86-022-23509140; e-mail guannj@nankai.edu.cn.

10.1021/jp805724s CCC: $40.75
Published on Web 10/15/2008

SCHEME 1: Proposed Mechanism for Formation of Fe_3O_4 from $FeCl_3 \cdot 6H_2O$ in the Presence of β-Cyclodextrins

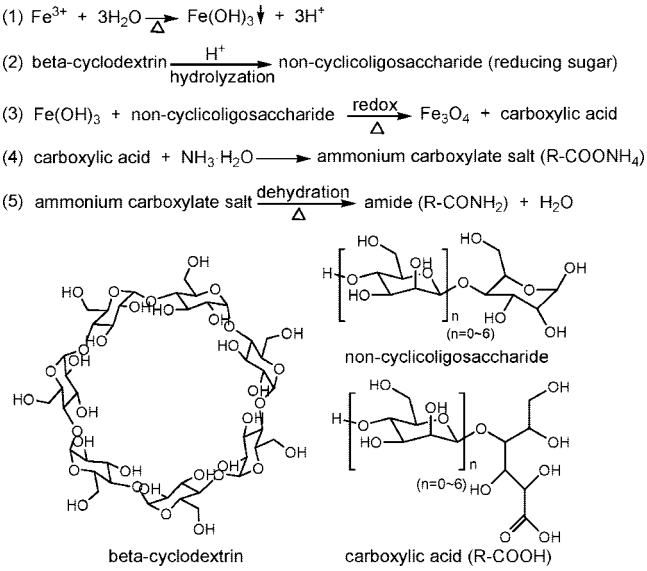

assembly of CD and the hydroxy groups are also known to mediate compatibility with an inorganic-oxide matrix through hydrogen bonding.[26] Yang and co-workers[27] utilized α-CD as an inclusion host to modify the surface of oleic acid-coated magnetite nanoparticles to "pull" them from hydrophobic solvents to aqueous phase. Ohta and co-workers[28] and Xia et al.[29] used a similar inclusion complex mechanism to form spherical magnetite aggregates with controllable size by changing the concentration of β-CD. Gedanken and co-workers[30] reported on the preparation of magnetite nanorods by sonochemical oxidation of the aqueous solution of iron(II) acetate in the presence of β-CD, in which they thought β-CD acted only as a size-stabilizing agent. Moreover, CD were also used to coat the as-synthesized magnetite nanoparticles as a surfactant to make the particles more biocompatible.[31,32] However, to the best of our knowledge, except for the above-mentioned function of CD related to the synthesis of magnetite, it remains unknown to make use of CD and the hydrolysis product of CD at the same time to help the formation of magnetite (Fe_3O_4) from a single Fe(III) precursor.

In this study, the pure phase magnetite (Fe_3O_4) nanoparticles were successfully synthesized from $FeCl_3 \cdot 6H_2O$ alone, in the presence of β-CD but without any purgation or protection by nitrogen or argon. The size of the magnetic nanoparticles could be controlled easily by tailoring the concentration of β-CD. Its success for the synthesis of pure Fe_3O_4 from $FeCl_3 \cdot 6H_2O$ alone could be ascribed (see Scheme 1) to in situ formation of some reducing sugars from β-CD, which are known to be nonreducing sugars without any aldehyde, ketone, hemiacetal, or hemiketal group.[28] The particular effect mechanism of β-CD-assisted synthesis of magnetite nanoparticles was studied in detail by ^{1}H NMR, Fourier transform infrared spectroscopic (FT-IR), X-ray photoelectron spectroscopic (XPS), and thermogravimetric (TG) analyses. Magnetization measurements indicated that all the particles were of single magnetic domain and superparamagnetic.

2. Experimental Section

2.1. Materials. The chemical reagents used in this work are ferric chloride hexahydrate ($FeCl_3 \cdot 6H_2O$), β-cyclodextrin (β-CD), and ammonia solution (($NH_3 \cdot H_2O$), 25%). All chemical reagents are of analytical grade.

2.2. Synthesis of Pure Magnetite (Fe_3O_4) Nanoparticles in the Presence of β-CD. In a typical experimental procedure, β-CD was dissolved in deionized water (1 mol) at a constant temperature of 60 °C, and then $FeCl_3 \cdot 6H_2O$ (2 mmol) was added with vigorous stirring. The pH of the solution was adjusted to ca. 10 by dropwise addition of 25% ammonia solution. After vigorous stirring was carried on for about 30 min, the obtained mixture was transferred into a Teflon-lined stainless steel autoclave (25 mL capacity) for crystallization at 150 °C for 6 h. After the autoclave was naturally cooled to room temperature, the product was isolated from the liquid phase by centrifugation and then thoroughly washed with deionized water three times to remove possible excess surfactant remainders. The final product was dried at 60 °C overnight and appeared as a fine dark-black powder. In this work, the effect of β-CD concentration (with molar ratio of $FeCl_3 \cdot 6H_2O$ to β-CD of 4:5, 4:3, and 2:1, respectively) on the size and dispersion of magnetite particles was mainly investigated, and the as-synthesized nanoparticles were denoted as samples a, b, and c with particle sizes of 4, 12, and 17 nm. Although the β-CD concentration greatly influenced the particle size, the effects were not linear owing to the complex nature of the growth process. Moreover, when the β-CD concentration was decreased further, no pure phase magnetite nanoparticles larger than 17 nm average diameter were synthesized. Furthermore, it should be mentioned that the control experiment without the addition of β-CD, with a similar reaction procedure as mentioned above, led to the formation of pure hematite (α-Fe_2O_3) instead of magnetite (Fe_3O_4).

2.3. Characterization. X-ray powder diffraction (XRD) patterns of the dry samples were performed at room temperature on a Rigaku D/max 2500 diffractometer with a graphite monochromator and Cu Kα radiation ($\lambda = 0.154$ nm). Typically, the data were collected from 10° to 80° with a resolution of 0.2°. The average crystallite size was estimated from the Debye−Scherrer equation, $D = K\lambda/(\beta \cos \theta)$, where D is the average crystal diameter, β is the corrected peak width (full width at half-maximum), K is a constant related the shape of the crystallites ($K = 0.94$), λ is the wavelength of the X-rays employed, and θ is the diffraction angle. The width of the diffraction peak with the highest intensity was selected for the calculation. Standard and high-resolution transmission electron microscopy (TEM and HRTEM) measurements were performed on a Philips Tecnai F20 microscope, 200 kV, equipped with a field emission gun. All samples subjected to TEM measurements were ultrasonically dispersed in alcohol and drop-cast onto copper grids. Raman spectra were measured by a Renishaw inVia Raman microscope at room temperature with the 514 nm line of an Ar laser as an excitation source. ^{1}H NMR spectra were acquired on a Varian Mercury Vx 300 with sample solutions in dimethyl sulfoxide-d_6 (DMSO-d_6). Fourier transform infrared (FT-IR) spectra were recorded on a Bruker Vector 22 FT-IR spectrophotometer by use of KBr pellets. Thermogravimetric analysis (TGA) was performed on a Rigaku thermogravimetry−differential thermal analysis (TG-DTA) analyzer with a heating rate of 6 °C/min in the presence of N_2 gas. X-ray photoelectron spectroscopy (XPS) measurements were acquired on a PHI 5300 ESCA XPS spectrometer with monochromatic Mg KR excitation. Zero-field cooled/field cooled (ZFC/FC) measurements were performed on a superconducting quantum interference device (SQUID) magnetometer (Quantum Design model MPMS XL-7) between 5 and 300 K. Magnetization study

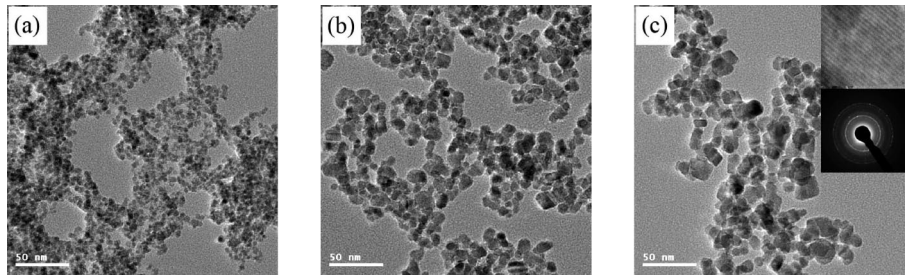

Figure 1. TEM images of as-synthesized iron oxide nanoparticles with various β-CD concentrations (molar ratio of $FeCl_3 \cdot 6H_2O$ to β-CD was 4:5, 4:3, and 2:1, respectively, for samples a, b, and c). The HRTEM image and ED pattern are shown as insets in panel c.

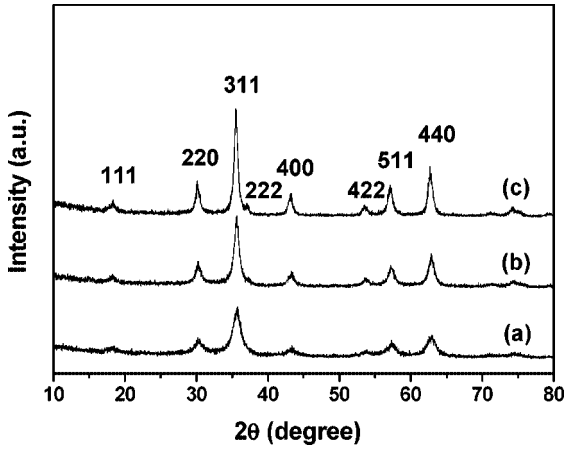

Figure 2. Power XRD patterns of as-synthesized magnetite nanoparticles with various β-CD concentrations (molar ratio of $FeCl_3 \cdot 6H_2O$ to β-CD was 4:5, 4:3, and 2:1, respectively, for samples a, b, and c).

was performed at room temperature on a LDJ 9600 VSM magnetometer.

3. Results and Discussion

3.1. Particle Morphology and Structural Characterization. Figure 1 shows typical TEM images of three iron oxide nanoparticle samples obtained with various β-CD concentration, all of which show rather uniform sizes and shapes. Their average particle sizes are found to increase with the decreasing concentration of β-CD and are calculated as 4.0 ± 1.2, 12.2 ± 2.1, and 17.1 ± 2.7 nm, respectively, based on the counting of about 100 particles. The enhanced β-CD concentration also leads to more homogeneous dispersion of nanoparticles. Smaller-sized nanoparticles display roughly spherical shapes, whereas most of the larger nanoparticles exhibit cubic shapes. This indicates that the shape and size of the iron oxides are strongly related to the concentration of β-CD. High-resolution TEM (inset in Figure 1c) shows well-defined lattice planes with good crystallinity, based on which the interplanar distance of 0.48 nm was calculated and assigned to the characteristic (111) spinel planes of magnetite (Fe_3O_4) particles.[14] The electron diffraction (ED) pattern presents clear and well-defined rings that can be indexed to magnetite structure.[20] The reflections characteristic of maghemite (γ-Fe_2O_3) are not observed.

The crystalline structures of samples a, b, and c were further determined by powder XRD patterns (Figure 2). The diffraction patterns and relative intensities of all diffraction peaks match well with those from the JCPDS card (19-0629) for pure magnetite.[17] No other iron oxide or hydroxide phase was observed. The broad peaks suggest the nanocrystallite nature of the magnetite particles. With the increase of β-CD concentration, there is continuous broadening of each XRD pattern peak,

TABLE 1: Average Grain Size[a] and Crystallite Size[b] of Magnetite Nanoparticles Prepared with Varying β-CD Concentrations

sample	molar ratio of $FeCl_3 \cdot 6H_2O$ to β-CD	size from TEM (nm)	size from XRD (nm)
a	4:5	4.0 ± 1.2	4.1
b	4:3	12.2 ± 2.1	12.3
c	2:1	17.1 ± 2.7	16.8

[a] Deduced from TEM observations. [b] From XRD results.

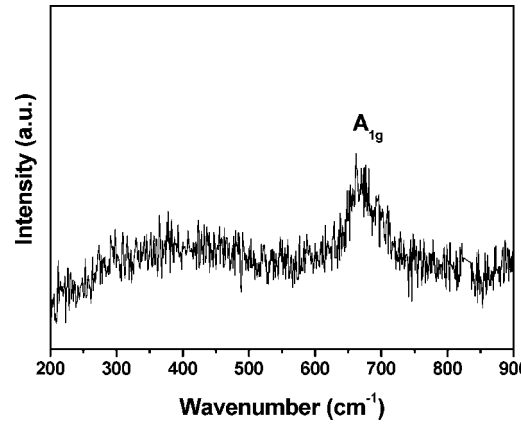

Figure 3. Raman spectra of magnetite sample b (4:3 molar ratio of $FeCl_3 \cdot 6H_2O$ to β-CD).

which is attributed to the decrease in particle size. By use of Debye−Scherrer equation for the full width at half-maximum (fwhm) of the (311) reflection, the average particle sizes were calculated to be 4.1, 12.3, and 16.8 nm, respectively, which are quite close to the TEM results (see Table 1). This means that all the as-synthesized magnetite particles are single-crystal and their size control could be achieved by changing the β-CD concentration, which is different from the seed-mediated growth method.[18]

The XRD patterns of magnetite (Fe_3O_4) and maghemite (γ-Fe_2O_3) are very similar,[33] except that a few low-intensity diffractions at $2\theta = 23.8°$ (210) and 26.1 ° (211) are present only for maghemite structure. In this study, it is very important to make sure that the as-synthesized iron oxide is pure magnetite for understanding the synthesis mechanism. In Figure 2, the (210) and (211) X-ray peaks of maghemite were not observed, but it is not enough to exclude the possible presence of maghemite phase because their intensities are lower than 5%. However, Raman spectroscopy can also differentiate the iron oxide phases,[34] since magnetite has a main band centered at 668 cm^{-1}, whereas maghemite shows broad structures around 700, 500, and 350 cm^{-1}.[35] Figure 3 illustrates the Raman spectra measured for magnetite sample b: only the absorption band at ca. 670 cm^{-1} (A_{1g}) can be observed and assigned to the

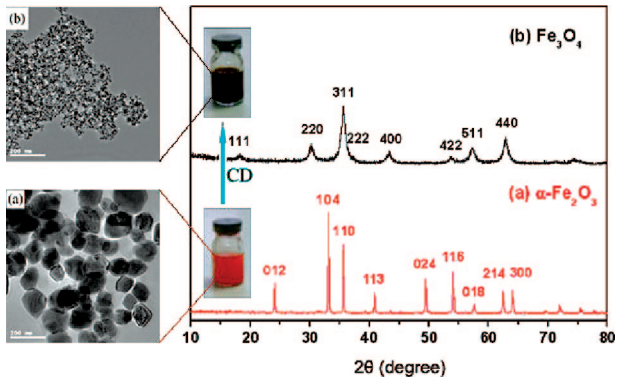

Figure 4. XRD, TEM, and digital images of the as-synthesized particles (b) with β-CD and (a) without β-CD; similar reaction procedures were used.

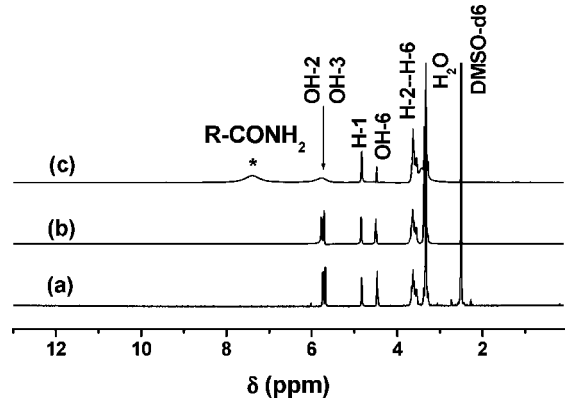

Figure 5. ^{1}H NMR spectra in dimethyl sulfoxide-d_6 (DMSO-d_6) of (a) raw β-CD; (b) organic remainders from a similar reaction process to sample b but without the addition of $FeCl_3 \cdot 6H_2O$; (c) organic remainders of sample b after removal of the particles by centrifugation.

characteristic band of pure magnetite. It means that the obtained iron oxide nanoparticles here are pure magnetite phase without any maghemite phase present. The broadened Raman peaks suggest the nanocrystalline nature of Fe_3O_4, in accordance with the XRD and TEM results.

3.2. Effect Mechanism of β-CD. It should be pointed out that the current synthetic approach is the first successful β-CD-assisted synthesis of pure magnetite nanoparticles from a single iron precursor of $FeCl_3 \cdot 6H_2O$ and without any purgation or protection by nitrogen or argon. The particle size could be controlled easily from 4 to 17 nm by tailoring the concentration of β-CD, in which β-CD acted as a coating agent. On the other hand, the β-CD adopted here belong to nonreducing sugar without aldehyde, ketone, hemiacetal, or hemiketal group; from a single iron precursor of $FeCl_3 \cdot 6H_2O$ and without any reducing atmosphere in our synthetic approach, pure Fe_3O_4 phase was obtained, so a certain kind of reducing agent should exist to ensure the formation of Fe_3O_4 with the mixed valences of Fe(II) and Fe(III). Therefore, more systematic examinations should be carried out to determine the exact effect mechanism of β-CD on the formation of pure magnetite nanoparticles from $FeCl_3 \cdot 6H_2O$ alone and on their size and morphology control.

First, the preparation procedure without the addition of β-CD was investigated as a contrast. As shown in Figure 4, the as-synthesized particles without the addition of β-CD can be identified as α-Fe_2O_3 (JCPDS 33-0664, Figure 4a) instead of Fe_3O_4. Comparatively, the XRD diffraction peaks of the dark-black magnetite sample obtained with β-CD are typically broader (Figure 4b). On the basis of the Scherrer equation, their average particle sizes can be calculated as ca.120 nm (α-Fe_2O_3) and 12.3 nm (Fe_3O_4), separately. Their different size distributions can also be demonstrated by their TEM images, where the hematite particles synthesized free of β-CD are heterogeneously dispersed with much larger size than the magnetite particles prepared with β-CD. All of above results indicate that the addition of β-CD is necessary for the formation of much smaller magnetite nanoparticles instead of larger hematite particles. It should be mentioned that in the system β-CD acts as a bifunctional surfactant: both as the precursor of the reducing agent, which partly reduces Fe^{3+} ions to Fe^{2+} ions and inhibits the reoxidation of the as-synthesized Fe_3O_4 particles, and as the coating agent, which leads to the formation of much smaller encapsulated nanoparticles and prohibits the agglomeration of particles.

The formation of Fe_3O_4 demonstrates that the Fe^{3+} ion precursors have been partly reduced to Fe^{2+} ions in the reaction process. However, β-CD, a nonreducing sugar, lacks reducing ability, so it is reasonable to deduce that the reducing species should originate from the hydrolysis product of β-CD. To confirm this supposition, ^{1}H NMR spectroscopy was used to analyze the organic remainders of the reaction solution after removal of the particles by centrifugation. Since the remainders of organic reaction for all samples synthesized with β-CD are very similar, only the sample b system will be discussed here (see Figure 5c). In Figure 5b, without the addition of $FeCl_3 \cdot 6H_2O$ (blank experiment), ^{1}H NMR spectroscopy of the remainders shows only the presence of β-CD, which means β-CD does not change without $FeCl_3 \cdot 6H_2O$. However, one new kind of amide (R-$CONH_2$)[36] with a broad N−H absorption between δ7 and δ8 was formed in the preparation solution of sample b (Figure 5c) in addition to the excess β-CD (unchanged peaks of H-1−H-6, OH-2, OH-3, and OH-6).[37] It means that, in our preparation system, hydrolysis of β-CD occurred and caused the formation of a certain reducing intermediate species that reduced Fe^{3+} into Fe_3O_4 accompanied by the ultimate organic production of amide (R-$CONH_2$).

It has been reported that hydrolysis of β-CD at the proper pH value (pH < 7), temperature, and metallic ion concentration could lead to the formation of various reducing sugars that are noncyclic oligosaccharides, such as glucose,[38] maltotetrose,[39] and maltoheptaose,[40] by breaking up one or more indican bonds. Similarly, in our work, the pH value of the reaction solution greatly decreased from ca. 7 to ca. 3 due to the hydrolysis of Fe^{3+} ions. Both the hydrothermal reaction temperature and the presence of some amounts of Fe^{3+} ions under our experimental conditions are also similar to the reaction conditions in which β-CD could hydrolyze to some kinds of noncyclic oligosaccharides.[38] One direct proof for the hydrolysis of β-CD to some kind of reducing intermediate species of noncyclic oligosaccharides is the FT-IR spectra (see Figure 6b) collected from the reaction intermediate solution (reaction time of only 2 h). It can be clearly observed that two low-frequency C−H stretching absorptions around 2750 and 2840 cm^{-1} and one C═O stretching around 1730 cm^{-1} have appeared, which suggests the existence of the aldehyde (-CHO)[36] group in any noncyclic oligosaccharides. Here the formed aldehyde group acted as the reducing species for partial reduction of Fe^{3+} ions to Fe^{2+} ions to produce Fe_3O_4 accompanied by self-oxidation into carboxylic acid (R-COOH). Subsequently, carboxylic acid could react with $NH_3 \cdot H_2O$ used for the pH value adjustment to form ammonium carboxylate salt (R-$COONH_4$), which could be further dehydrated above 100 °C to produce amide (R-

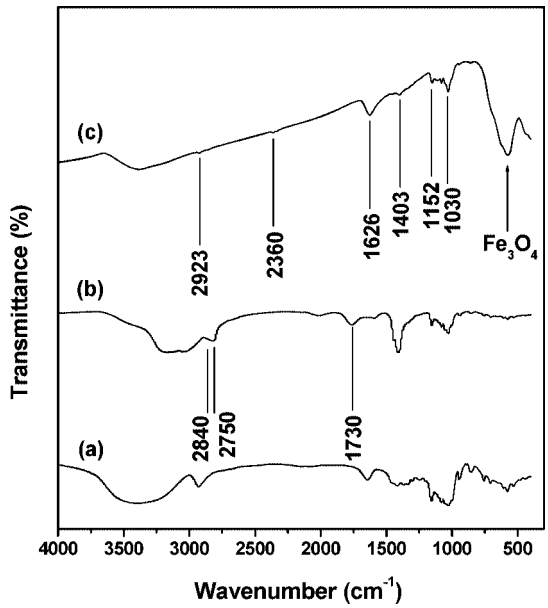

Figure 6. FT-IR spectra of (a) raw β-CD, (b) intermediate organic product in the synthesis of sample b when reaction time is only 2 h, and (c) as-synthesized magnetite nanoparticles, sample b.

$CONH_2$), as identified in ^1H NMR spectroscopy (Figure 5c). In accordance with these results and analyses, a possible mechanism leading to the formation of Fe_3O_4 from a single iron precursor of $FeCl_3 \cdot 6H_2O$ in the presence of β-CD is proposed in Scheme 1.

In fact, the hydrolysis of β-CD is rather complex. Therefore, Scheme 1 cannot depict all the reactions that may take place. Only those related to the formation of Fe_3O_4 are shown. First, $FeCl_3 \cdot 6H_2O$ is hydrolyzed to form ferric oxide or hydroxide releasing H^+ protons and decreasing the pH value of solution (reaction 1). Subsequently, under suitable reaction environments such as pH value, temperature, and iron ion concentration, the hydrolysis of β-CD produces the reducing sugar (noncyclic oligosaccharide) (reaction 2). Then a redox process between ferric oxide or hydroxide and noncyclic oligosaccharide proceeded and was accompanied by crystallization of magnetite and formation of carboxylic acid (reaction 3). Finally, $NH_3 \cdot H_2O$ reacted with carboxylic acid to form ammonium carboxylate salt (reaction 4), which was further dehydrated to produce amide at temperatures above 100 °C (reaction 5). As a whole, β-CD continually self-decomposed into enough reducing sugar (noncyclic oligosaccharide), leading to the final formation of pure Fe_3O_4 phase. Summarily, the as-adopted β-CD functioned as the precursor of reducing sugars that induced the formation of magnetite alone from a single iron precursor of $FeCl_3 \cdot 6H_2O$, even though β-CD lacks reducing ability by itself. That also explains the absence of any purgation or protection by nitrogen or argon in our system very well.

Another function of β-CD is to act as a coating agent to prevent growth and aggregation of the particles. As is known, conventional hydrothermal synthesis usually leads to growth and aggregation of bulk particles as demonstrated in Figure 4a due to the nucleation and subsequent growth of particles, which often take place in an uncontrolled manner.[23] In contrast, well-dispersed nanoscale magnetite particles with uniform particle sizes could be obtained by the β-CD-assisted synthesis method herein. It is proposed that β-CD, with multiple hydroxyl groups, can chelate ferric oxide or hydroxide and adsorb onto certain crystal planes as a coating agent to provide steric hindrance,[41] similar to conventional surfactants and capping ligands. This

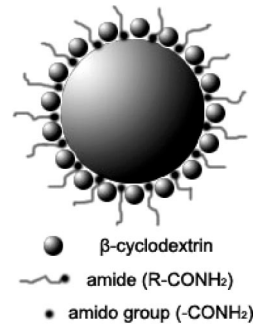

Figure 7. Schematic illustration of β-cyclodextrin and amide-coating Fe_3O_4 nanoparticles. Note that the structures of the coating agents on the surface of the nanoparticles are simplified.

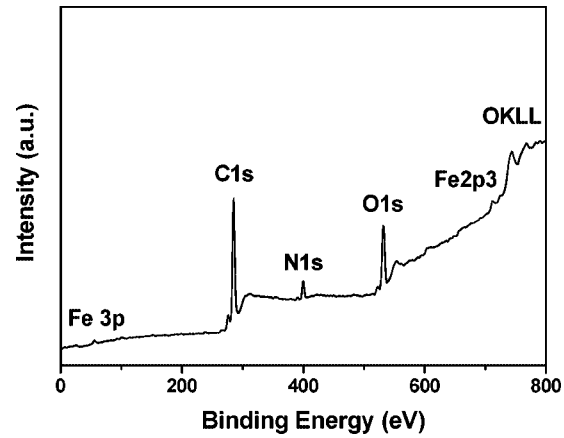

Figure 8. XPS spectrum of as-synthesized magnetite nanoparticle sample b.

complexation leads to the nucleation and subsequent growth of a nanocrystalline phase in a controlled manner, resulting in an improvement in the uniformity of crystallite size and morphology. On the other hand, the final organic product amide (see Scheme 1) with an amido group (-$CONH_2$) can also chelate the magnetite particle as a coating agent with the same effect as β-CD in the formation of nanoscale particles.[42] This means that the small amount of surfactant (including β-CD and amide, as shown in Figure 7) plays a critical role in modifying the particle size and crystalline characteristics.

The coating effect of β-CD on the surface of magnetite nanoparticles was shown by typical FT-IR spectroscopy (Figure 6c) of the as-synthesized magnetite sample b. Two characteristic bands at around 2923 cm^{-1} (C−H stretching) and 1152−1030 cm^{-1} (C−O stretching) in the spectrum confirmed the attachment of β-CD on the particle surfaces.[43] A weak absorption band at 1403 cm^{-1} of C−N stretching came from the partial coating of amide, which was demonstrated by ^1H NMR spectroscopy.[36] The broad band centered at 3406 cm^{-1} could be assigned to hydrogen-bonded O−H stretching vibration arising from surface hydroxyl group on nanoparticles and adsorbed β-CD and water.[43] In addition, the absorption bands at 1626 and 2360 cm^{-1} referred to the vibration of remainder H_2O and adsorbed CO_2 in the sample, respectively.[43,44] A strong absorption band at 576 cm^{-1} is related to the vibration of the Fe−O functional group, which further corroborated that the phase of as-prepared particles is magnetite.[42] Figure 8 shows the XPS spectra for encapsulated magnetite nanoparticles. The appearance of the characteristic two peaks of Fe 2p and O 1s is typical for iron oxide, while the peaks ascribed to C 1s, O 1s, and N 1s at expected positions further indicate the existence of β-CD and amide coating on the surface of the magnetite nanoparticles.[45]

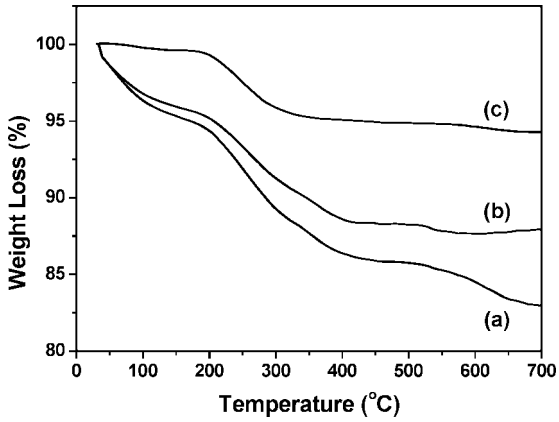

Figure 9. TGA curves of the as-synthesized magnetite nanoparticles with various β-CD concentrations performed under nitrogen atmosphere (molar ratio of $FeCl_3 \cdot 6H_2O$ to β-CD was 4:5, 4:3, and 2:1, respectively, for samples a, b, and c).

More proof of the coating of β-CD on the surface of magnetite nanoparticles comes from their TG analysis measurements, which were performed under nitrogen atmosphere in order to minimize the mass increase due to the oxidation of Fe^{2+} ions and only allow the surfactants to decompose thermally. As demonstrated in Figure 9, all the TG analysis data of samples a, b, and c synthesized with different concentrations of β-CD show similar weight loss curves that are mainly composed of two processes. The first weight loss below 200 °C should be attributed to the dehydration of the powders, and the second one, in the temperature region of 200−400 °C with an inflection point at about 204 °C, corresponds to desorption and subsequent evaporation of the coating agents, including β-CD and small amounts of amide as shown in Figure 6c.[20] As far as all the samples are concerned, the percentage of the second weight loss increases with the enhanced initial concentration of β-CD, which indicates that a larger concentration of β-CD favors the formation of smaller nanoparticles with larger amounts of coating agents.

The distinct coating amount of surfactants will have a dissimilar effect on the nucleation and growth of particles, so the size and morphology of magnetite nanoparticles could be controlled in this way, as observed in Figure 1. In view of the strong coordination ability of the hydroxyl groups of β-CD, the rapid hydrolysis of Fe^{3+} ions, and the supramolecular self-assembly of β-CD, the rate of nucleation of the Fe species should be very high, leading to the formation of ultrathin homogeneous crystal nuclei on the composites of β-CD assembly. On the other hand, these composites act as supramolecular coating agents of Fe species and greatly suppress the growth and aggregation of Fe nuclei due to steric hindrance. The rate of crystallization of magnetite is thus decreased. The higher the concentration of β-CD, the stronger the steric hindrance becomes and the smaller the size of the formed particle is. Moreover, the mineralizers (hydroxyl ions) are adsorbed onto the hydrophobic interior of β-CD,[46] thus further slowing the crystallization process of Fe species during hydrothermal synthesis. As a result of all the above factors, rapid nucleation and slow crystallization of magnetite were obtained in the presence of β-CD, which led to the formation of uniform and ultrathin magnetite nanoparticles whose particle size could be controlled easily by adjusting the concentration of β-CD.

3.3. Magnetic Measurements. The temperature dependence of zero-field cooling (ZFC) and field cooling (FC) magnetization in an applied magnetic field of 20 Oe between 5 and 300 K for samples a, b, and c is presented in Figure 10. For samples b and c, ZFC and FC curves do not coincide up to

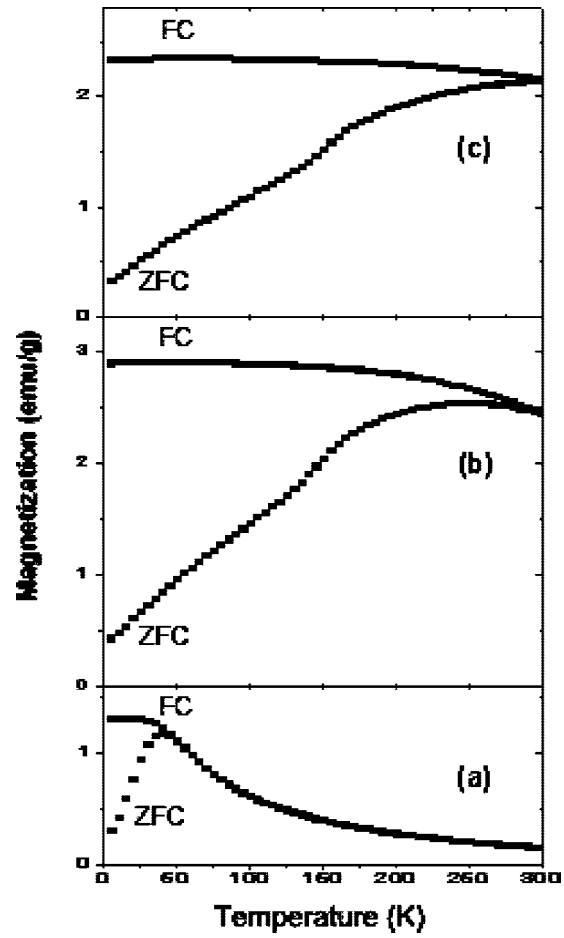

Figure 10. Temperature dependence of zero-field cooling (ZFC) and field cooling (FC) magnetization measured for magnetite samples a, b, and c (molar ratio of $FeCl_3 \cdot 6H_2O$ to β-CD was 4:5, 4:3, and 2:1, respectively).

300 K, and for sample a, ZFC and FC curves depart from each other below ∼60 K. When the samples are cooled at zero magnetic field, the total magnetization of the particles will be zero since the magnetic moments of individual particles are randomly oriented for Brownian motion. An external magnetic field energetically favors the moments of the individual particles to reorient along the applied field at low temperature. With increasing temperature, more and more particles reorient their magnetization with the external field and the total magnetization increases and reaches a maximum in the ZFC curve, which is characterized in general as the blocking temperature (T_B).[22] At this temperature, the transition from ferromagnetic to superparamagnetic behavior is observed. The superparamagnet is an assembly of magnetically aligned moments in a single-domain fine particle. The main characteristic of a superparamagnetic particle is that thermal energy is enough to make the magnetization of the particle oscillate rapidly, so that the observed net magnetization at room temperature is zero. This happens because of the small value of their magnetic anisotropy energy, which is proportional to particle volume. The blocking temperatures of samples a, b, and c are found to be 40, ∼248, and ∼290 K, respectively. The different blocking temperatures are attributed to different sizes and the existence of a broadened distribution of energy barriers.[20]

Magnetization properties of the as-prepared magnetite nanoparticles were investigated at room temperature by measuring magnetization curves (Figure 11). All the samples

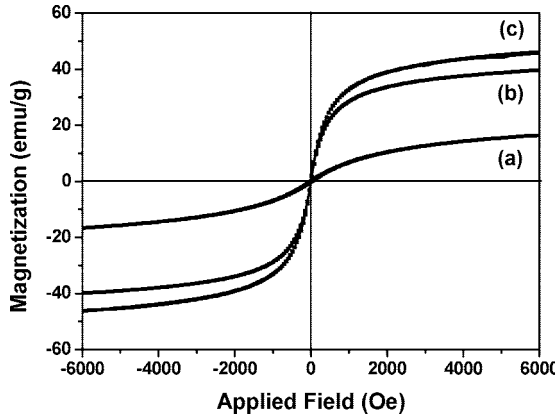

Figure 11. Magnetization curves at room temperature of magnetite samples a, b, and c (molar ratio of $FeCl_3 \cdot 6H_2O$ to β-CD was 4:5, 4:3, and 2:1, respectively).

demonstrate typical superparamagnetic behavior with negligible coercivity and remanence, in accordance with the theory that superparamagnetic behavior is often observed at room temperature with magnetite particles smaller than 20 nm.[14] The samples exhibit saturation magnetization (M_s) of 16.43, 39.86, and 46.41 emu/g, respectively, with increasing particle size, which should be mainly attributed to the difference in both particle size and organic shells concentration as evidenced from TGA experiments (Figure 9). Compared to the theoretical value of the bulk Fe_3O_4 (92 emu/g),[22] a decrease in saturation magnetization is often observed with nanoparticles and is attributed to the surface contribution: spin canting, surface disorder, stoichiometry deviation, cation distribution, and adsorbed species including water and organic shells.[14] In addition, saturation magnetization values of our samples are lower than those of similarly sized nanoparticles prepared by other methods,[18] which might be caused by the noncollinear spin structure, which originated from the pinning of the surface spins and coated surfactant, resulting in the reduction of magnetic moment in such nanoparticles.[47]

4. Conclusions

Here we introduced the β-CD-assisted synthesis of superparamagnetic magnetite nanoparticles from a single Fe(III) precursor of $FeCl_3 \cdot 6H_2O$, free of protection by nitrogen or argon. In the presence of β-CD, homogeneous nanoparticles with average particle sizes from 4 to 17 nm can be achieved. The functions of β-CD were discussed in detail; it is known to act both as the precursor of the reducing agent and as a coating agent. The former function explains the formation mechanism of pure Fe_3O_4 from a single Fe(III) source, and the latter function is responsible for the formation and size control of ultrathin nano-Fe_3O_4. The route is a simple, economical, and environmentally friendly one and can be expected to extend into the preparation of other oxides with complex metal valences.

Acknowledgment. This research was financially supported by National Basic Research Program of China (also called 973, Grant 2003CB615801), National Natural Science Foundation of China (Grants 20573059 and 20777039), International S&T Cooperation Program of China (Grant 2007DFA90720), and Fok Ying Tung Education Foundation (Grant 114039).

References and Notes

(1) Lu, A. H.; Salabas, E. L.; Schüth, F. *Angew. Chem., Int. Ed.* **2007**, *46*, 1222.

(2) Jeong, U.; Teng, X. W.; Wang, Y.; Yang, H.; Xia, Y. N. *Adv. Mater.* **2007**, *19*, 33.

(3) Raj, K.; Moskowitz, R. *J. Magn. Magn. Mater.* **1990**, *85*, 233.

(4) Arico, A. S.; Bruce, P.; Scrosati, B.; Tarascon, J. M.; Schalkwijk, W. V. *Nat. Mater.* **2005**, *4*, 366.

(5) Hu, A. G.; Yee, G. T.; Lin, W. B. *J. Am. Chem. Soc.* **2005**, *127*, 12486.

(6) Sen, T.; Sebastianelli, A.; Bruce, I. J. *J. Am. Chem. Soc.* **2006**, *128*, 7130.

(7) Lee, H.; Lee, E.; Kim, D. K.; Jang, N. K.; Jeong, Y. Y.; Jon, S. Y. *J. Am. Chem. Soc.* **2006**, *128*, 7383.

(8) Roullin, V. G.; Deverre, J. R.; Lemaire, L.; Hindre, F.; Julienne, M. C. V.; Vienet, R.; Benoit, J. P. *Eur. J. Pharm. Biopharm.* **2002**, *53*, 293.

(9) Kim, D. K.; Zhang, Y.; Kehr, J.; Klason, T.; Bjelke, B.; Muhammed, M. *J. Magn. Magn. Mater.* **2001**, *225*, 256.

(10) Kang, Y. S.; Risbud, S.; Rabolt, J. F.; Stroeve, P. *Chem. Mater.* **1996**, *8*, 2209.

(11) Lee, Y.; Lee, J.; Bae, C. J.; Park, J. G.; Noh, H. J.; Park, J. H.; Hyeon, T. *Adv. Funct. Mater.* **2005**, *15*, 503.

(12) Kumar, R. V.; Diamant, Y.; Gedanken, A. *Chem. Mater.* **2000**, *12*, 2301.

(13) Wang, X.; Zhuang, J.; Peng, Q.; Li, Y. D. *Nature* **2005**, *437*, 121.

(14) Daou, T. J.; Pourroy, G.; Begin-Colin, S.; Greneche, J. M.; Ulhaq-Bouillet, C.; Legare, P.; Bernhardt, P.; Leuvrey, C.; Rogez, G. *Chem. Mater.* **2006**, *18*, 4399.

(15) Rockenberger, J.; Scher, E. C.; Alivisatos, P. A. *J. Am. Chem.Soc.* **1999**, *121*, 11595.

(16) Hyeon, T.; Lee, S. S.; Park, J.; Chung, Y.; Na, H. B. *J. Am. Chem. Soc.* **2001**, *123*, 12798.

(17) Sun, S. H.; Zeng, H.; Robinson, D. B.; Raoux, S.; Rice, P. M.; Wang, S. X.; Li, G. X. *J. Am. Chem. Soc.* **2004**, *126*, 273.

(18) Li, Z.; Chen, H.; Bao, H. B.; Gao, M. Y. *Chem. Mater.* **2004**, *16*, 1391.

(19) Jana, N. R.; Chen, Y. F.; Peng, X. G. *Chem. Mater.* **2004**, *16*, 3931.

(20) Hou, Y. L.; Yu, J. F.; Gao, S. *J. Mater. Chem.* **2003**, *13*, 1983.

(21) Liu, J. C.; Qin, G. W.; Raveendram, P.; Ikushima, Y. *Chem.—Eur. J.* **2006**, *12*, 2131.

(22) Si, S.; Kotal, A.; Mandal, T. K.; Giri, S.; Nakamura, H.; Kohara, T. *Chem. Mater.* **2004**, *16*, 3489.

(23) Cushing, B. L.; Kolesnichenko, V. L.; O'Connor, C. J. *Chem. Rev.* **2004**, *104*, 3893.

(24) Mnger, W. S.; Jacob, J.; Gessler, K.; Steiner, T.; Hoffmann, D.; Sanbe, H.; Koizumi, K.; Smith, S. M.; Takaha, T. *Chem. Rev.* **1998**, *98*, 1787.

(25) Engeldinger, E.; Armspach, D.; Matt, D. *Chem. Rev.* **2003**, *103*, 4147.

(26) Li, L. D.; Sun, X. H.; Yang, Y. L.; Guan, N. J.; Zhang, F. X. *Chem.—Asian J.* **2006**, *1*, 664.

(27) Wang, Y.; Wong, J. F.; Teng, X. W.; Lin, X. Z.; Yang, H. *Nano Lett.* **2003**, *3*, 1555.

(28) Hou, Y. L.; Kondoh, H.; Shimojo, M.; Sako, E. O.; Ozaki, N.; Kogure, T.; Ohta, T. *J. Phys. Chem. B* **2005**, *109*, 4845.

(29) Xia, H. B.; Yi, J. B.; Foo, P. S.; Liu, B. H. *Chem. Mater.* **2007**, *19*, 4087.

(30) Kumar, R. V.; Koltypin, Y.; Xu, X. N.; Yeshurun, Y.; Gedanken, A.; Felner, I. *J. Appl. Phys.* **2001**, *89*, 6324.

(31) Racuciu, M.; Creanga, D. E.; Sulitanu, N.; Badescu, V. *Appl. Phys. A: Mater. Sci. Process.* **2007**, *89*, 565.

(32) Bocanegra-Diaz, A.; Mohallem, N. D. S.; Novak, M. A.; Sinisterra, R. D. *J. Magn. Magn. Mater.* **2004**, *272*, 2395.

(33) Pinna, N.; Grancharov, S.; Beato, P.; Bonville, P.; Antonietti, M.; Niederberger, M. *Chem. Mater.* **2005**, *17*, 3044.

(34) Zhou, Z. H.; Wang, J.; Liu, X.; Chan, H. S. O. *J. Mater. Chem.* **2001**, *11*, 1704.

(35) Bersani, D.; Lottici, P, P.; Montenero, A. *J. Raman Spectrosc.* **1999**, *30*, 355.

(36) Wade, L. G., Jr. *Organic Chemistry*; Pearson Prentice Hall: Upper Saddle River, NJ, 2003.

(37) Schneider, H. J.; Hacket, F.; Rudiger, V.; Ikeda, H. *Chem. Rev.* **1998**, *98*, 1755.

(38) Tewari, Y. B.; Goldberg, R. N.; Sato, M. *Carbohydr. Res.* **1997**, *301*, 11.

(39) Anindyawati, T.; Melliawati, R.; Ito, K.; Iizuka, M.; Minamiura, N. *Biosci. Biotechnol. Biochem.* **1998**, *62*, 1351.

(40) Yang, S. J.; Lee, H. S.; Kim, J. W.; Lee, M. H.; Auh, J. H.; Lee, B. H.; Park, K. H. *Carbohydr. Res.* **2006**, *341*, 420.

(41) Tang, J.; Redl, F.; Zhu, Y.; Siegrist, T.; Brus, L. E.; Steigerwald, M. L. *Nano Lett.* **2005**, *5*, 543.
(42) Wang, L. Y.; Bao, J.; Wang, L.; Zhang, F.; Li, Y. D. *Chem.—Eur. J.* **2006**, *12*, 6341.
(43) Cai, W.; Wan, J. Q. *J. Colloid Interface Sci.* **2007**, *305*, 366.
(44) Rajh, T.; Chen, L. X.; Lukas, K.; Liu, T.; Thurnauer, M. C.; Tiede, D. M. *J. Phys. Chem. B* **2002**, *106*, 10543.
(45) Xuan, S. H.; Hao, L. Y.; Jiang, W. Q.; Gong, X. L.; Hu, Y.; Chen, Z. Y. *Nanotechnology* **2007**, *18*, 035602.
(46) Zangi, R.; Engberts, J. B. F. N. *J. Am. Chem. Soc.* **2005**, *127*, 2272.
(47) Kodama, R. H.; Berkowitz, A. E.; McNiff, E. J.; Foner, S. *Phys. Rev. Lett.* **1996**, *77*, 394.

JP805724S